

Nonequilibrium transport through magnetic vibrating molecules

P. Roura-Bas,¹ L. Tosi,² and A. A. Aligia²

¹*Departamento de Física, Centro Atómico Constituyentes, Comisión Nacional de Energía Atómica, Buenos Aires, Argentina*

²*Centro Atómico Bariloche and Instituto Balseiro, Comisión Nacional de Energía Atómica, 8400 Bariloche, Argentina*

(Received 20 December 2012; published 28 May 2013)

We calculate the nonequilibrium conductance through a molecule or a quantum dot in which the occupation of the relevant electronic level is coupled with intensity λ to a phonon mode and also to two conducting leads. The system is described by the Anderson-Holstein Hamiltonian. We solve the problem using the Keldysh formalism and the noncrossing approximation for both the electron-electron and the electron-phonon interactions. We obtain a moderate decrease of the Kondo temperature T_K with λ for fixed renormalized energy of the localized level \tilde{E}_d . The meaning and value of \tilde{E}_d are discussed. The spectral density of localized electrons shows, in addition to the Kondo peak of width $2T_K$, satellites of this peak shifted by multiples of the phonon frequency ω_0 . The nonequilibrium conductance as a function of bias voltage V_b at small temperatures also displays peaks at multiples of ω_0 in addition to the central dominant Kondo peak near $V_b = 0$.

DOI: 10.1103/PhysRevB.87.195136

PACS number(s): 71.38.-k, 73.63.-b, 85.65.+h, 72.15.Qm

I. INTRODUCTION

Single-molecule electronic devices, such as molecular transistors, are being extensively studied because they offer perspectives for further miniaturization of electronic circuits with important potential applications.^{1–5} In addition, they provide realizations of fundamental issues in condensed matter physics. Examples are the spin- $\frac{1}{2}$ (Refs. 6–9) and spin-1 (Refs. 10–12) Kondo effect, which lead to an increased conductance at low temperatures with different behaviors. In C_{60} quantum dots, quantum phase transitions involving partially Kondo screened spin-1 molecular states were induced changing the gate voltage.^{10,12} These experiments could be explained semiquantitatively using extensions of the impurity Anderson model treated with either the numerical renormalization group^{12,13} (NRG) or with the noncrossing approximation (NCA).^{12,14,15} This approximation allows calculations out of equilibrium and in particular at finite bias voltage. While these calculations did not include phonons, the latter are known to play an important role for molecular transistors under suitable conditions.^{16–20} For example (as a rather special case), evidence for a coupling between the center-of-mass motion of the C_{60} molecules with the hopping to the leads was found in a single- C_{60} transistor with gold leads.¹⁶ Phonon effects were also observed in other systems. For example, transport through adatoms on Si surfaces takes place in particular situations, only when vibrations are excited,¹⁸ and the differential conductance $G = dI/dV_b$ through conjugated molecules shows peaks when the applied bias voltage V_b matches multiples of a phonon frequency.¹⁷

In some molecular transistors based on organometallic molecules, an anomalous gate-voltage dependence of the transport properties has been reported.^{6,7,21} In particular, Yu *et al.* found that the Kondo temperature T_K depends weakly on the applied gate voltage and shows a rapid increase only close to the charge degeneracy points.²¹ Such behavior is inconsistent with the usual theory based on the impurity Anderson model, but could be explained using the Anderson-Holstein model,²² which is an extension of the former to include a single-phonon mode coupled linearly with the charge in the molecule. At equilibrium ($V_b \rightarrow 0$), the

Anderson-Holstein model has been studied with NRG,^{22–24} Monte Carlo,²⁵ a mean-field approach,²⁶ NCA decoupling phonons,²⁷ an interpolative perturbative approach,²⁸ and the equation-of-motion (EOM) method.²⁹

For finite bias voltage V_b , the interplay of Kondo and vibrations has been studied using a real-time diagrammatic technique,³⁰ functional renormalization group after a Schrieffer-Wolf transformation,³¹ EOM decoupling phonons,³² imaginary-time quantum Monte Carlo plus analytical continuation,³³ and NCA decoupling phonons.^{34,35} For spinless electrons, for which no Kondo screening is possible, the nonequilibrium case was analyzed by Monreal *et al.*³⁶ using EOM and an interpolative self-energy approximation which is exact for small λ and in the atomic limit, following similar ideas as those used to study the pure electronic problem out of equilibrium for small Coulomb repulsion U .^{37,38}

Previous NCA approaches^{27,34,35} used a Lang-Firsov canonical transformation, and then decouple the phonons in a mean-field approach. A problem with this decoupling is that for a fixed renormalized localized level \tilde{E}_d , predicts that the Kondo temperature changes exponentially with the electron-phonon coupling λ , which is actually not the case.^{23,29,31}

In this work, we extend the NCA as applied to the infinite- U limit of the Anderson model^{39,40} to include explicitly the effect of the phonons. For the case of one doublet, comparison of NCA with NRG results⁴¹ shows that the NCA describes rather well the Kondo physics. The leading behavior of the differential conductance for small voltage and temperature⁴² agrees with alternative Fermi-liquid approaches,^{43,44} and the temperature dependence of the conductance practically coincides with the NRG result over several decades of temperature.⁴² A shortcoming of the NCA is that, at very low temperatures, it introduces an artificial spike at the Fermi energy in the spectral density when the ground state of the system without coupling to the leads is nondegenerate, although the thermodynamic properties continue to be well described.³⁹ Another limitation of the method is that it is restricted to temperatures above $\sim T_K/20$, where T_K is the Kondo temperature. An advantage of the method over the EOM is that it is a conserving approximation and gives

the right exponential dependence of T_K on the energy of the localized state E_d , while the EOM has a factor of the order of 1 in the exponent.⁴⁵ While the NRG is more accurate at low energies, the NCA has a comparative advantage that it can be extended rather easily to nonequilibrium situations. In addition, it is able to capture features at high energies such as peaks in the spectral density out of the Fermi level, which might be broadened or lost in NRG calculations.⁴⁶ An example is the plateau at intermediate temperatures observed in transport through C_{60} molecules for gate voltages for which triplet states are important,^{10,12} which was missed in early NRG studies, but captured by the NCA.^{14,15} More recent NRG calculations, using tricks to improve the resolution,⁴⁷ have confirmed this plateau.¹²

The paper is organized as follows. In Sec. II, we describe the model and discuss the renormalization of the level energy due to electron-phonon interaction. In Sec. III, we explain the modifications of the NCA nonequilibrium formalism to include the phonon mode and the electron-phonon interaction. In Sec. IV, we show our main results. Section V contains the summary and a short discussion. Some details are left to the Appendix.

II. MODEL

The model describes one level of a molecule at an energy E_d , with Coulomb repulsion U between electrons at the same level, coupled to two conducting leads and a Holstein mode of frequency ω_0 .²²⁻³⁶ The Hamiltonian is

$$H = [E_d + \lambda(a^\dagger + a)]n_d + Un_{d\uparrow}n_{d\downarrow} + \sum_{vk\sigma} \epsilon_k^v c_{vk\sigma}^\dagger c_{vk\sigma} + \sum_{vk\sigma} (V_k^v d_\sigma^\dagger c_{vk\sigma} + \text{H.c.}) + \omega_0 a^\dagger a, \quad (1)$$

where $n_d = \sum_\sigma n_{d\sigma}$, $n_{d\sigma} = d_\sigma^\dagger d_\sigma$, d_σ^\dagger creates an electron with spin σ at the relevant state of a molecule (or quantum dot), a^\dagger creates the Holstein phonon mode, λ is the electron-phonon coupling, $c_{vk\sigma}^\dagger$ creates a conduction electron at the left ($v = L$) or right ($v = R$) lead, and V_k^v describes the hopping elements between the leads and the molecular state.

For each energy $\epsilon_k^L = \epsilon_k^R$ for which there are states at the left and the right, only the linear combination $V_k^L c_{Lk\sigma} + V_k^R c_{Rk\sigma}$ hybridizes with the molecular state. Thus, the model is effectively a one-channel Anderson-Holstein model.

A. Effective purely electronic model

For $\lambda = 0$, the model reduces to the ordinary impurity Anderson model and its main properties are well known.⁴⁸ In particular, in the Kondo regime $\epsilon_F - E_d \gg V_K$ where ϵ_F is the Fermi energy and K denotes k, v , the characteristic low-energy scale is given by the Kondo temperature $T_K \sim \exp[-1/(\rho J)]$, where ρ is the spectral density of the conduction states for given spin, and for $U \rightarrow \infty$ (which corresponds to our NCA calculations) $J = 2|V_K|^2/(\epsilon_F - E_d)$ for constant V_K . The half width at half maximum of the peak near the Fermi energy in the spectral density $\rho(\omega)$ is proportional to T_K , as well as the corresponding widths of the peaks of the conductance $G(T, V_b) = dI/dV_b$ as a function of temperature T and bias voltage V_b near $T = V_b = 0$ (I is the current).⁴⁹ Any of these

half widths might be used as a definition of T_K . Here, we use that of $\rho(\omega)$.

If the electrons could be decoupled from the phonons in some approximation, one might expect that an effective purely electronic model H_{eff} of the form of the ordinary impurity Anderson model, but with renormalized parameters \tilde{E}_d, \tilde{V}_K describes the electronic motion, leading to a renormalized Kondo temperature $T_K \sim \exp\{-1/[2\rho|\tilde{V}_K|^2/(\epsilon_F - \tilde{E}_d)]\}$. How T_K varies with λ will be discussed in Sec. IV A. For this discussion, it is necessary to define \tilde{E}_d in some way. In the rest of this section, we discuss this definition and some limits of the model.

The model given by Eq. (1) can be solved exactly for $V_k^v = V_K = 0$. In this case, the total number of electrons in the molecule n_d is a good quantum number and the electron-phonon interaction λ can be eliminated by a simple shift in the phonon operator $\beta^\dagger = a^\dagger + \hat{c}$, where \hat{c} is an operator that depends on n_d . This simply reflects the fact that the equilibrium position of the normal-mode coordinate depends on the occupation. It is easy to see that for each n_d , one has

$$\hat{c} = -\frac{\lambda}{\omega_0} n_d, \quad \Delta E = -\frac{(\lambda n_d)^2}{\omega_0}, \quad (2)$$

where ΔE is the energy gain due to the electron-phonon interaction. Then, for $V_k^v = 0$, the Hamiltonian takes the form

$$H_0 = \tilde{E}_d^0 n_d + \tilde{U} n_{d\uparrow} n_{d\downarrow} + \sum_{vk\sigma} \epsilon_k^v c_{vk\sigma}^\dagger c_{vk\sigma} + \omega_0 \left(a^\dagger + \frac{\lambda}{\omega_0} n_d \right) \left(a + \frac{\lambda}{\omega_0} n_d \right), \quad (3)$$

where the subscript 0 reminds us that (for the moment) $V_K = 0$ and the renormalized level energy and Coulomb repulsion are

$$\tilde{E}_d^0 = E_d - \frac{\lambda^2}{\omega_0}, \quad \tilde{U} = U - 2\frac{\lambda^2}{\omega_0}. \quad (4)$$

For very large ω_0 , the last term of Eq. (3) can be neglected and H_0 reduces to a purely electronic model with effective parameters. In this antiadiabatic approximation,⁵⁰ when one includes the hybridization term, it becomes exponentially reduced due to the fact that it mixes states with different n_d , and the scalar product of the phonon wave functions with different equilibrium positions leads to a factor $\tilde{V}_K/V_K = \exp[-(\lambda/\omega_0)^2/2]$.²⁸ Thus, the effective Hamiltonian for $\omega_0 \rightarrow \infty$ becomes

$$H_{\text{eff}} = \tilde{E}_d n_d + \tilde{U} n_{d\uparrow} n_{d\downarrow} + \sum_{vk\sigma} \epsilon_k^v c_{vk\sigma}^\dagger c_{vk\sigma} + (\tilde{V}_K d_\sigma^\dagger c_{K\sigma} + \text{H.c.}) \quad (5)$$

with $\tilde{E}_d = \tilde{E}_d^0$.

The limit $\omega_0 \rightarrow \infty$ is, however, not realistic. In the general case, the electron-phonon interaction can also be eliminated using a Lang-Firsov unitary transformation.^{51,52} The price to pay is that \tilde{V}_K includes exponentials of phonon operators which are usually treated in a decoupling approximation, which as in the antiadiabatic limit, usually leads to an exponential dependence of T_K on λ for fixed \tilde{E}_d^0 , which is not found in more elaborate treatments.^{23,29,31}

In any case, if the antiadiabatic limit, or a decoupling approximation leading to a purely electronic Hamiltonian H_{eff} has to be abandoned, one might ask if the renormalized level energy \tilde{E}_d is still given by \tilde{E}_d^0 [first Eq. (4)] in a more elaborate treatment. This equation comes as a result of optimizing the energy neglecting the hybridization, leading to a shift given by the first Eq. (2) in the equilibrium position of the oscillator. One expects that for large hybridization, a smaller shift giving rise to a smaller gain of elastic energy but a larger gain in hybridization energy is more convenient. Here, we define

$$\tilde{E}_d = \frac{\langle g|P_1 H P_1|g\rangle}{\langle g|P_1|g\rangle} - \frac{\langle g|P_0 H P_0|g\rangle}{\langle g|P_0|g\rangle}, \quad (6)$$

where $|g\rangle$ is the ground state and P_n is a projector on the subspace with $n_d = n$. We have estimated \tilde{E}_d using a simple variational approximation, where \hat{c} is replaced by a constant c obtained minimizing the ground-state energy. The details are given in the Appendix. The first Eq. (A4) shows that the phonon shift has in fact smaller magnitude than λ/ω_0 and Eq. (A6) gives a smaller shift of \tilde{E}_d than the corresponding one Eq. (4) for zero hybridization. However, the variational approach is too simple and we do not pretend this result to be quantitatively valid. Qualitative aspects will be discussed in Sec. IV B.

III. FORMALISM

Here, we describe briefly the extension of the noncrossing approximation (NCA) applied before for the Anderson model with infinite onsite repulsion out of equilibrium^{39,40} to include the phonons. As before,^{39,40} a slave boson b and two slave fermions f_σ are introduced. $b^\dagger|0\rangle$ represents the state without particles at the molecular level, and the physical fermions are given by $d_\sigma^\dagger = f_\sigma^\dagger b$. These pseudoparticles should satisfy the constraint

$$b^\dagger b + \sum_\sigma f_\sigma^\dagger f_\sigma = Q, \quad (7)$$

with $Q = 1$, which is enforced introducing a Lagrange multiplier Λ . A usual trick is to take $\Lambda \rightarrow \infty$ at the end, to make the projection on the physical subspace $Q = 1$.³⁹ The quantities of interest can be expressed in terms of the lesser and greater Keldysh Green's functions for the pseudoparticles, which for stationary nonequilibrium processes are defined as^{52,53}

$$\begin{aligned} G_\sigma^<(t-t') &= +i\langle f_\sigma^\dagger(t')f_\sigma(t)\rangle, & D^<(t-t') &= -i\langle b^\dagger(t')b(t)\rangle, \\ G_\sigma^>(t-t') &= -i\langle f_\sigma(t)f_\sigma^\dagger(t')\rangle, & D^>(t-t') &= -i\langle b(t)b^\dagger(t')\rangle. \end{aligned} \quad (8)$$

These Green's functions correspond to the interacting (dressed) propagators. In the present case, we have to add the Green's functions of the phonons:

$$\begin{aligned} A^<(t-t') &= -i\langle a^\dagger(t')a(t)\rangle = -in(\omega_0)\exp[-i(t-t')\omega_0], \\ A^>(t-t') &= -i\langle a(t)a^\dagger(t')\rangle = -i[n(\omega_0) + 1] \\ &\quad \times \exp[-i(t-t')\omega_0]. \end{aligned} \quad (9)$$

Here, we have written in the last member, the result for noninteracting phonons, where $n(\omega) = [\exp(\omega/kT) - 1]^{-1}$ is

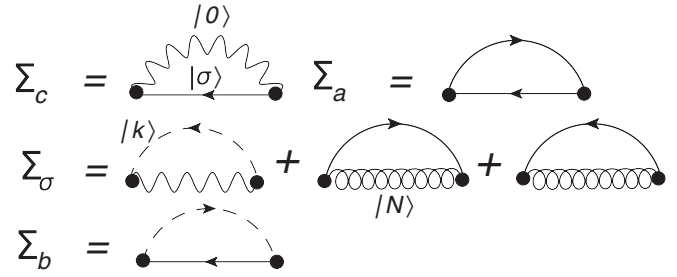


FIG. 1. Self-energies obtained within the NCA for the electron-electron and electron-phonon coupling. Full straight (wavy) lines correspond to fermion (boson) pseudoparticle propagators. Dashed lines represent conduction electrons and curly lines phonons. The first two diagrams vanish in the NCA treatment (see text). The diagram for the Hartree term is in Fig. 1(c) of Ref. 28.

the Bose-Einstein distribution function. This is because the diagram of order λ^2 , which corrects the noninteracting result, contains two pseudofermion lines (see diagram for Σ_a in Fig. 1). These diagrams vanish in the limit $\Lambda \rightarrow \infty$ (as the corresponding one for the self-energy of the conduction electrons). Therefore, the phonon Green's functions are not corrected within the NCA.

The retarded and advanced fermion Green's functions are $G_\sigma^r(t) = \theta(t)[G_\sigma^>(t) - G_\sigma^<(t)]$, $G_\sigma^a = G_\sigma^r + G_\sigma^< - G_\sigma^>$, and similarly for the bosonic Green's functions. Within the NCA, the self-energy diagrams are calculated as in second order in the boson-fermion interaction $\sum_{\nu k\sigma} (V_k^\nu f_\sigma^\dagger b c_{\nu k\sigma} + \text{H.c.})$ and the electron-phonon interaction $\lambda(a^\dagger + a) \sum_\sigma f_\sigma^\dagger f_\sigma$, but replacing the bare propagators by the dressed ones, which are determined self-consistently. This is equivalent to a partial sum of diagrams to all orders in perturbation theory (all the noncrossing ones).

Most of the self-consistent integral equations take the same form as those of the case $\lambda = 0$.³⁹ In Fig. 1, the diagrams for the different self-energies are shown. The only difference is that the lesser and greater self-energies for the pseudofermions include the electron-phonon corrections $\Sigma_{\text{ph},\sigma}^{\lessgtr}$ given below, and the retarded self-energy contains the Hartree term $E_H = -2 \sum_\sigma \langle f_\sigma^\dagger f_\sigma \rangle \lambda^2 / \omega_0$, which is independent of frequency.²⁸ However, this term vanishes for $\Lambda \rightarrow \infty$.

The corrections of Σ^{\lessgtr} due to phonons are

$$\Sigma_{\text{ph},\sigma}^{\lessgtr}(\omega) = \frac{i\lambda^2}{2\pi} \int d\omega' G_\sigma^{\lessgtr}(\omega + \omega') [A^{\lessgtr}(-\omega') + A^{\gtrless}(\omega')]. \quad (10)$$

Adding this to the contribution of the hybridization and using Eqs. (9), one obtains

$$\begin{aligned} \Sigma_\sigma^<(\omega) &= \lambda^2 \{ n(\omega_0) G_\sigma^<(\omega - \omega_0) + [n(\omega_0) + 1] G_\sigma^<(\omega + \omega_0) \} \\ &\quad - \sum_\nu \Gamma_\nu \int \frac{d\omega'}{2\pi} f_\nu(\omega - \omega') D^<(\omega'), \end{aligned} \quad (11)$$

$$\begin{aligned} \Sigma_\sigma^>(\omega) &= \lambda^2 \{ n(\omega_0) G_\sigma^>(\omega + \omega_0) + [n(\omega_0) + 1] G_\sigma^>(\omega - \omega_0) \} \\ &\quad + \sum_\nu \Gamma_\nu \int \frac{d\omega'}{2\pi} [1 - f_\nu(\omega - \omega')] D^>(\omega'), \end{aligned} \quad (12)$$

where $f_\nu(\omega) = \{\exp[(\omega - \mu_\nu)/kT] + 1\}^{-1}$, μ_ν is the chemical potential of the lead ν , and

$$\Gamma_\nu(\omega) = 2\pi \sum_k |V_k^\nu|^2 \delta(\omega - \epsilon_k^\nu) \quad (13)$$

assumed independent of ω .

With the exception of Eqs. (11) and (12), the rest of the formalism, including the equation for the current,^{54,55} has the same form as for the case without phonons, explained in detail in previous works,^{39,40} and we do not reproduce them here.

IV. NUMERICAL RESULTS

For the numerical calculations, we assume a constant density of states per spin of the leads ρ between $-D$ and D . We take the unit of energy as the frequency of the phonon $\omega_0 = 1$ and $D = 10$. We also take $\Gamma_L = \Gamma_R = \Delta$, where Δ , called the resonance level width, is half the width at half maximum of the spectral density of states in the noninteracting case. Without loss of generality, we assume $\epsilon_F = 0$, where ϵ_F is the Fermi level of the leads without applied bias voltage V_b . For finite V_b we assume a symmetric voltage drop, leading to chemical potentials of the leads $\mu_L = eV_b/2$, $\mu_R = -eV_b/2$, unless otherwise stated. At the end of this section, the nonequilibrium conductance for a case with asymmetric voltage drop and Γ_ν is shown.

A. Spectral density

In order to test the NCA for the phonons, we represent in Fig. 2 the spectral density of the physical fermion $\rho_{d\sigma}(\omega)$ in the particular case of zero hybridization $V_k^\nu = 0$, for several values of the electron-phonon interaction λ , and compare it with the exact result.³⁶ We used a logarithmic scale to render

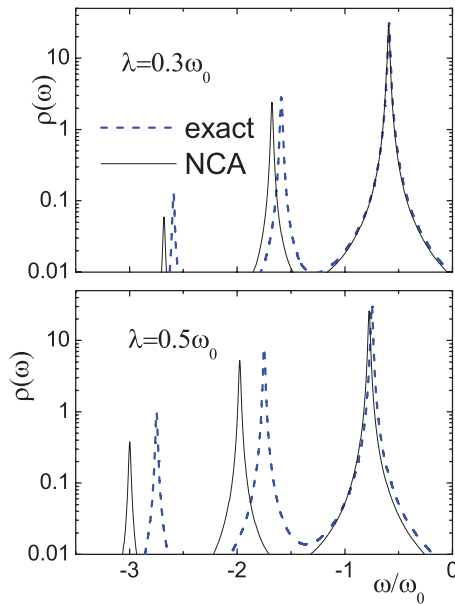


FIG. 2. (Color online) Comparison of NCA and exact results for the electronic spectral density per spin as a function of frequency for $V_k^\nu = 0$ and two values of λ . Other parameters are $\omega_0 = 1$, $E_d = -0.5$, and $T = 0$. An imaginary part of magnitude 0.01 was added to broaden the different peaks.

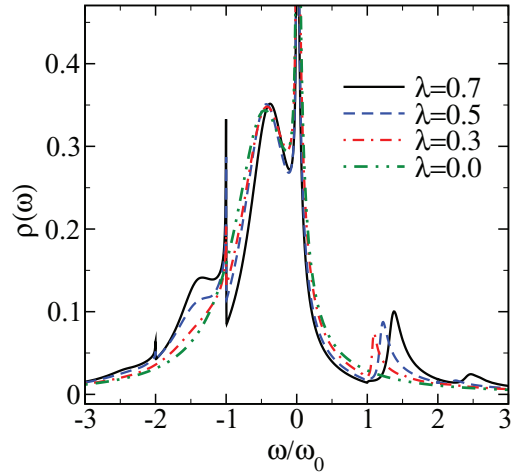


FIG. 3. (Color online) Electronic spectral density per spin as a function of frequency for temperatures well below the Kondo temperature, $\omega_0 = 1$, $\Delta = 0.2\omega_0$, $\tilde{E}_d^0 = -0.6$, and several values of λ .

visible the second replica of the main peak. For $V_k^\nu = 0$, n_d is a good quantum number and the problem can be solved exactly shifting the phonon operators depending on the occupation [see Eq. (3)]. This shift is not explicit in the NCA and it is not obvious that the correct physics is reproduced by the NCA for large λ . For $\tilde{E}_d < \epsilon_F = 0$, and temperature $T = 0$, one has $n_d = 1$. Thus, for infinite U as we assume, electrons can only be destroyed at the dot, and from the Lehman representation of the Green's function,⁵² it is clear that the spectral density has components only at negative frequencies. The main peak should be at $\omega = \tilde{E}_d$, where for $V_k^\nu = 0$, $\tilde{E}_d = \tilde{E}_d^0 = E_d - \lambda^2/\omega_0$, and its intensity is proportional to the square of the overlap between the ground state of the phonon wave functions for $n_d = 0$ (vacuum of phonon operator a) and $n_d = 1$ (vacuum of phonon operator β). There are more peaks shifted at lower energies by $n\omega_0$ with amplitude reduced by the overlap between the phonon ground state $|0_\beta\rangle$ for displaced phonons and the state $|n_a\rangle$ with n undisplaced phonons. As seen in the figure, the NCA reproduces very well the intensity and position of the main peak. For large λ , the position of this peak is slightly displaced from \tilde{E}_d . The shift λ^2/ω_0 is overestimated by about 5% for $\lambda = 0.5\omega_0$. The replicas are shifted to lower energies by the NCA, and their intensities are underestimated, but the NCA results remain semiquantitatively valid.

From now on, we discuss the results for $V_K \neq 0$. In Fig. 3, we show the spectral density of the physical fermion $\rho_{d\sigma}(\omega)$ for several values of the electron-phonon interaction λ . This figure has the same parameters as Fig. 6 of Ref. 29. The case $\lambda = 0$ is known, and one can see the usual narrow Kondo peak at the Fermi energy $\epsilon_F = 0$ and the broad charge-transfer peak near the energy \tilde{E}_d^0 . Both peaks clearly narrow with increasing λ . In addition, for $\lambda \neq 0$, both peaks have replicas with lower intensity shifted to negative frequencies by the phonon energy ω_0 . The replicas of the charge-transfer peak can just be interpreted as a broadening of the peaks shown in Fig. 2 as a consequence of the hybridization. In agreement with the EOM results of Ref. 29, we do not see replicas of the charge-transfer peak at positive frequencies. This is

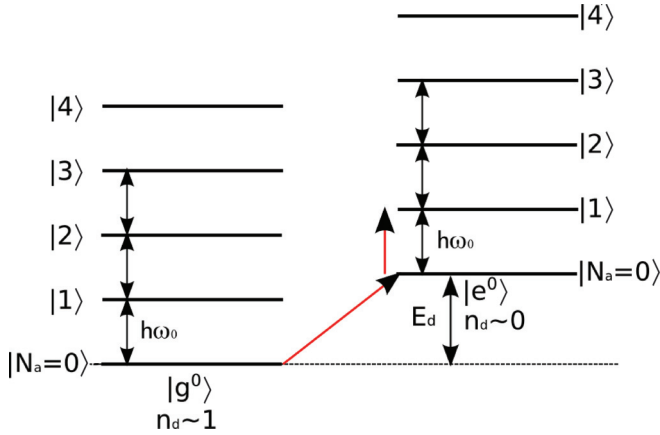


FIG. 4. (Color online) Scheme of the eigenstates of the system for $\lambda = 0$.

expected since this peak is due to annihilation of the occupied molecular state, and the spectral weight of this peak at positive frequencies (creation of this state) is very small for $U \rightarrow \infty$.

The replicas of the Kondo peak are more subtle. The Kondo peak is due to small charge fluctuations near the Fermi level and has contributions at both positive (creation of an electron at the localized level d_σ^\dagger) and negative (annihilation) frequencies. From the Lehman representation of the Green's function,⁵² the spectral density at $\omega = -\omega_0^*$, with ω_0^* near ω_0 , at zero temperature, is given by

$$\rho_{d\sigma}(-\omega_0^*) = \sum_e |\langle e | d_\sigma | g \rangle|^2 \delta(\omega_0^* - \epsilon_e), \quad (14)$$

where the states here are eigenstates of the complete Hamiltonian with electrons and phonons. $|g\rangle$ is the ground state and $|e\rangle$ are excited states with excitation energy ϵ_e (the difference between the energy of the state $|e\rangle$ and the ground-state energy E_g).

We denote as $|e_n^0\rangle$ the eigenstates for $\lambda = 0$ with n phonons added to the vacuum of the uncharged system ($|0_a\rangle$). $|g_0^0\rangle$ is the ground state for $\lambda = 0$ (see Fig. 4). Note that the electronic part of these states is independent of n , the phonon part of the energy is just $n\omega_0$ and $\langle e_n^0 | d_\sigma | g_n^0 \rangle$ is independent of n . We also call $|e_n^K\rangle$ the states $|e_n^0\rangle$ with very small electronic excitation energy and n phonons, which for $n = 0$ are responsible for the Kondo peak when $\lambda = 0$. For finite λ , the electron-phonon interaction mixes the states $|e_n^0\rangle$ and $|g_n^0\rangle$ (which are no longer eigenstates) with those with $n \pm 1$ phonons. In particular, the ground state $|g\rangle$ which for $\lambda = 0$ is $|g_0^0\rangle$ acquires some component of $|g_1^0\rangle$ (and smaller ones of $|g_n^0\rangle$). In turn, the states $|e\rangle$, which for $\lambda = 0$ are $|e_1^K\rangle$ (with energy near $E_g + \omega_0$), obtain some amount of $|e_0^K\rangle$ after turning on λ . These new components of the eigenstates lead to contributions to the matrix elements entering Eq. (14), which are similar to those of the Kondo peak and increase linearly with λ/ω_0 for small λ . In addition, the states $|e_0^0\rangle$ with energy near $E_g + \omega_0$ which have a large contribution to Eq. (14) for $\lambda = 0$ are expected to have a large mixing with $|e_1^K\rangle$ for finite λ because they have nearly the same energy. Both effects contribute to “translate” the electronic structure of the Kondo effect contained in $|e_n^K\rangle$ to the spectral density at $\omega \approx -n\omega_0$.

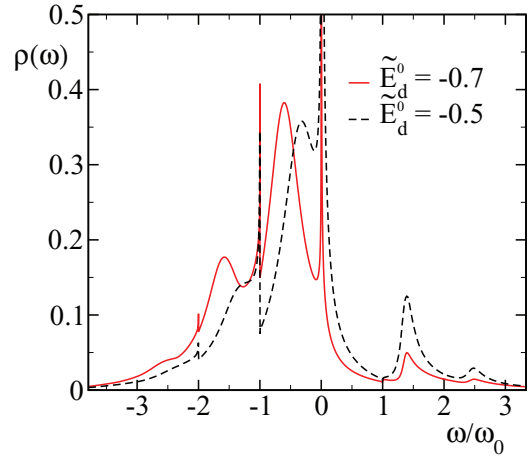


FIG. 5. (Color online) Electronic spectral density per spin as a function of frequency for $\Delta = 0.2\omega_0$, $\lambda = 0.7$, two values of \tilde{E}_d^0 , and temperatures well below the Kondo temperature.

An analogous reasoning can be followed for $\rho_{d\sigma}(\omega_0^*)$ (positive frequencies) changing d_σ by d_σ^\dagger in Eq. (14). For $\omega > \omega_0$, we obtain broad structures centered slightly below $\omega = n\omega_0 + \lambda^2/\omega_0$, with n integer. An observation of the first one ($n = 1$) indicates a small jump with increase in intensity at $\omega = \omega_0$ and a smooth evolution of the intensity with increasing ω . While we have not reached a complete understanding, several pieces of evidence (given below) indicate that this peak is a broadened replica of the Kondo peak. The shift in position with respect to ω_0 seems to be related with a loss of the energy gain ΔE [see Eq. (2)] in most of the excited states involved in the spectral decomposition of $d_\sigma^\dagger |g\rangle$. The broadening of the peak seems to be related in the uncertainty in the equilibrium position of the oscillator since n_d is not well defined. The position of this peak does not change with E_d as it might be expected for a feature related with the charge-transfer peak. This is shown in Fig. 5. From the figure, one also sees that as E_d decreases, the weight of this peak decreases. This is what is expected for a Kondo peak since its total weight is proportional to T_K , which decreases with decreasing E_d (see Sec. II A).

As discussed in more detail below, the evolution with temperature of the peak (see Fig. 6) also suggests that it is related with the Kondo one, which in contrast to the charge-transfer peak decreases in intensity as the temperature is increased. The replica of the Kondo peak at $\omega = -\omega_0$ is quite sharp. This is due to the fact explained in the previous section that the phonon spectral density is not renormalized within the NCA. Therefore, the softening and damping of the phonon mode due to its interaction with the electrons is absent. The phonon damping would broaden the replicas of the Kondo effect, in a more realistic description. However, it remains unclear to us why the replicas at negative frequencies are quite sharp, while those at positive frequency are broadened by some energy related with ΔE [see Eq. (2)]. Further studies with a technique that allows finite U might shed light on this issue.

The results displayed in Fig. 3 are qualitatively similar to those obtained previously using equations of motion (Fig. 6 of Ref. 29), but there are quantitative differences. The replica of

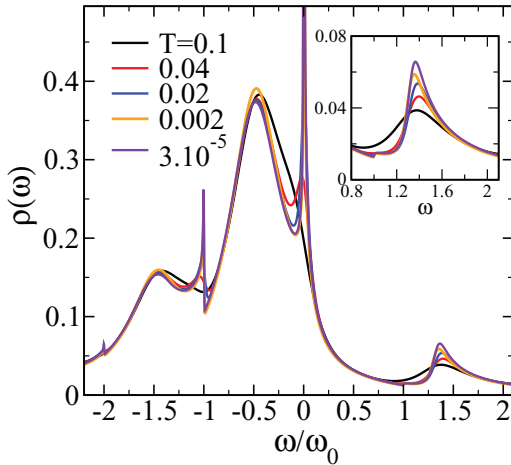


FIG. 6. (Color online) Electronic spectral density per spin as a function of frequency for $\tilde{E}_d^0 = -0.6$, $\Delta = 0.2\omega_0$, and $\lambda = 0.7$, and several temperatures. The inset is a detail of the peak near $\omega = \omega_0$.

the Kondo peak at ω near ω_0 is sharper in their work and located exactly at $\omega = \omega_0$. Instead, the replica of the Kondo peak near $-\omega_0$ seems absent in Ref. 29 and for larger λ , the spectral density seems to approach vanishing values near $\omega = \pm\omega_0$.

In Fig. 6 we show the evolution of the spectral density $\rho_{d\sigma}(\omega)$ with temperature. As it is known for the case with $\lambda = 0$, there is a strong temperature dependence of the peak at the Fermi energy (the Kondo peak) at temperatures of the order of the Kondo temperature T_K . We define T_K as the half width at half maximum of the Kondo peak at zero temperature. We observe a similar strong dependence of the satellite peaks near $\omega = \pm\omega_0$, suggesting that these peaks are replicas of the low-energy Kondo screening of the local magnetic moment combined with the effect of one virtual phonon. For example, while the intensity of the charge-transfer peak near \tilde{E}_d or its replica at $\tilde{E}_d - \omega_0$ hardly changes for temperatures of the order of T_K , the other peaks strongly lose intensity (for $\omega \sim 1.34\omega_0$) or disappear (for $\omega \sim 0, -\omega_0, -2\omega_0$) for $T = 0.1 > T_K \approx 0.01\omega_0$. In any case, the fact that a broad structure near $1.35 \sim \omega_0$ remains at that temperature is rather unexpected.

B. Dependence of T_K with the renormalized localized level

In presence of the electron-phonon interaction λ , for a fixed renormalized localized level \tilde{E}_d , T_K is expected to decrease with increasing λ due to the renormalization of the hybridization V . However, an exponential decrease (as predicted using simple decouplings of electrons and phonons) is not expected.^{23,29}

The inset of Fig. 7 displays our results for T_K as a function of λ for fixed \tilde{E}_d^0 . As in Ref. 29, we obtain a moderate decrease of T_K as the electron-phonon interaction λ increases. However, in our case we find a plateau between $0.6 < \lambda/\omega_0 < 0.7$, which at first sight seems surprising. We ascribe this effect to the fact that while \tilde{E}_d^0 is constant, the real effective localized level \tilde{E}_d increases with λ in this interval and there is a compensation of this effect (which tends to increase T_K) with the monotonic decrease of T_K with λ for fixed \tilde{E}_d . Following, we provide several arguments and calculations to support our conclusion.

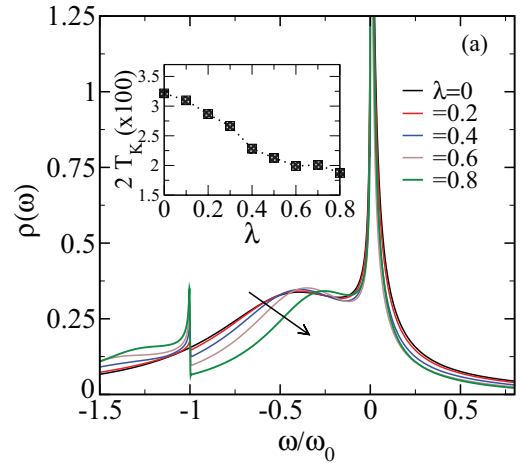


FIG. 7. (Color online) Spectral density for several values of λ , $\omega_0 = 1$, $\Delta = 0.2$, and $\tilde{E}_d^0 = -0.5$. The inset shows the width of the peak near $\omega = 0$ (two times the Kondo temperature T_K) as a function of λ .

One of them is that the maximum of the charge-transfer peak near $\omega \approx -0.4\omega_0$ in Fig. 7 moves to the right as lambda decreases. Note that the usual upward shift in the renormalized localized level $(\Delta/\pi)\ln(D/\Delta)$ calculated with poor man’s scaling⁵⁸ leads to a shift in the opposite direction because the effective resonant level width decreases.

In Fig. 8 we show $\Delta E_d = \tilde{E}_d - E_d^0$ as a function of λ with E_d calculated variationally as discussed in Sec. II A. With respect of the parameters of Fig. 7, we have multiplied Δ by a factor 2 because it leads approximately to the correct occupancy of the localized level when compared with NRG results.⁵⁹ Although the variational calculation can provide only qualitative results, one can see that it predicts the steepest increase of ΔE_d with λ near $\lambda/\omega_0 = 0.5$ and a saturation for larger λ , which is consistent with the existence of the plateau in Fig. 7. Further evidence for a shift in ΔE_d as a cause of this plateau is provided by the dependence of the occupancy of the localized level with λ (calculated with NCA). This is displayed in Fig. 9 and shows a behavior which is reminiscent of that of ΔE_d with a maximum near $\lambda/\omega_0 = 0.5$.

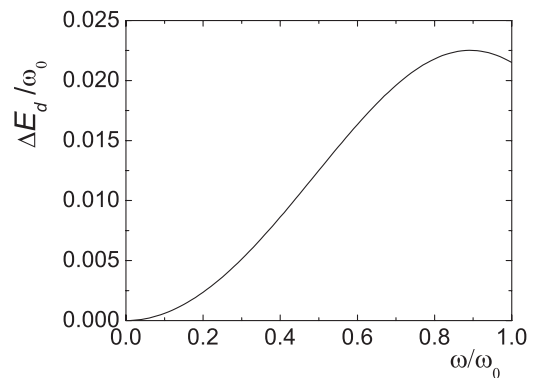


FIG. 8. Difference between the renormalized localized level and the bare one as a function of the electron-phonon interaction for $\omega_0 = 1$, $\Delta = 0.4$, and $\tilde{E}_d^0 = -0.5$.

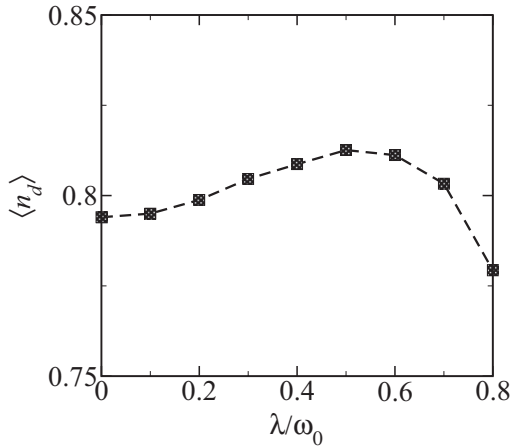


FIG. 9. Occupancy of the localized level as a function of electron-phonon interaction for the same parameters as Fig. 7.

As a final analysis of this situation, we have repeated several NCA calculations for each value of the electron-phonon interaction λ , shifting the bare level E_d in such a way that the maximum of the charge-transfer peak (near $\omega \approx -0.4\omega_0$ in Fig. 7) lies at the same position as for $\lambda = 0$, with an error smaller than a fraction of T_K . This procedure is very time consuming, but since the NCA is much superior than the variational calculation, it ensures that we are working at constant effective renormalized localized level \tilde{E}_d with reasonable accuracy.

The results are displayed in Fig. 10. In contrast to Fig. 7, one can see that the position of the charge-transfer peak remains constant, while it narrows as λ increases. Now, we obtain a nice monotonic decrease of T_K with λ as expected. Also, the occupancy of the localized level (not shown) has now a monotonic increase with λ from 0.79 for $\lambda = 0$ to 0.87 for $\lambda = 0.87\omega_0$.

A quantitative analysis of the narrowing of the charge-transfer peak is complicated by the presence of the side Kondo peaks and is beyond the scope of this work. In any case, it seems that the NCA does not give an exponential reduction of this

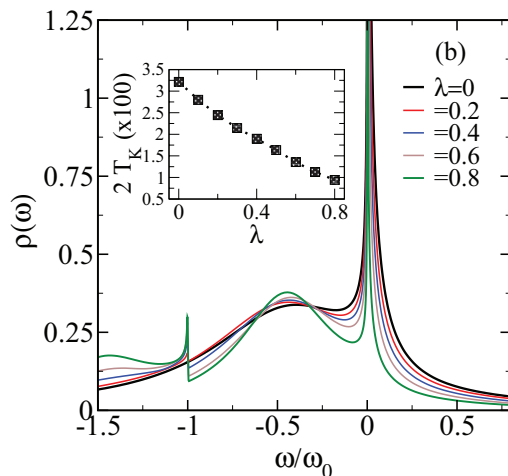


FIG. 10. (Color online) Same as Fig. 7 but with constant renormalized localized level $\tilde{E}_d = -0.5\omega_0$ (see text).

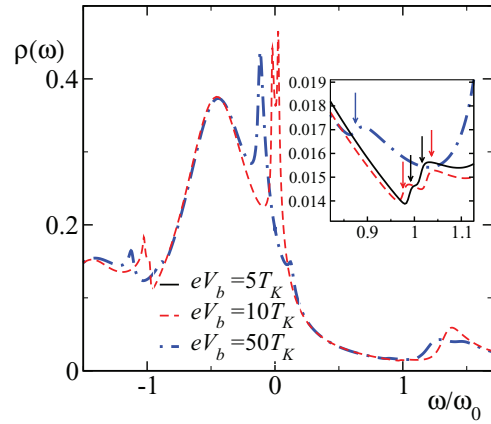


FIG. 11. (Color online) Electronic spectral density per spin as a function of frequency ω for $\Delta = 0.2\omega_0$, $\lambda = 0.7$, $\tilde{E}_d^0 = -0.3$, $T = 0.05T_K$, and several bias voltages. The inset shows details for $\omega \sim \omega_0$. The arrows indicate small steps at the left of the peak near $\omega \sim 1.35\omega_0$.

width with increasing electron-phonon interaction λ for fixed renormalized localized level \tilde{E}_d . Although an exponential renormalization factor is a common feature of strongly coupled electron-phonon couplings, as stressed by Hewson and Mayer, the exponential reduction does not in general occur in the strong-coupling regime of the model, but only in a certain parameter regime.²³

C. Nonequilibrium spectral density and conductance

In Fig. 11, the evolution of $\rho_{d\sigma}(\omega)$ with applied bias voltage V_b is displayed. We see that in addition of the known splitting of the Kondo peak with V_b ,^{39,40} also the replica of the Kondo peak near $\omega = -\omega_0$ splits, a fact which again supports the notion that this satellite peak is related with the Kondo peak at the Fermi energy. For $\omega \approx 1.35\omega_0$, a splitting also takes place, but only for bias voltage large enough so that eV_b overcomes the intrinsic width of this feature. The inset shows that the onset of this peak at $\omega = \omega_0$ is also split by the bias voltage, and the

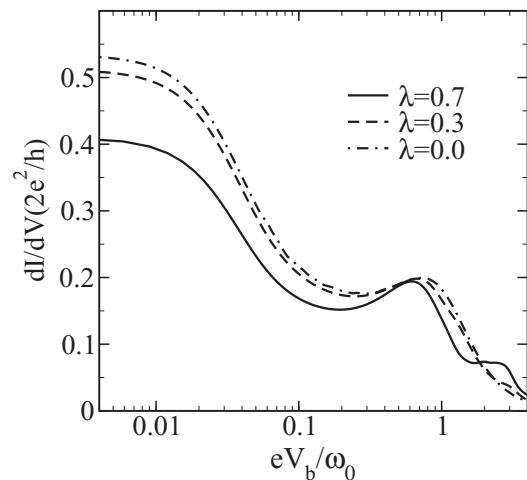


FIG. 12. Conductance as a function of the applied bias voltage for $\omega_0 = 1$, $T = 0.02$, $\tilde{E}_d^0 = -0.6$, $\Delta = 0.2$, and several values of λ .

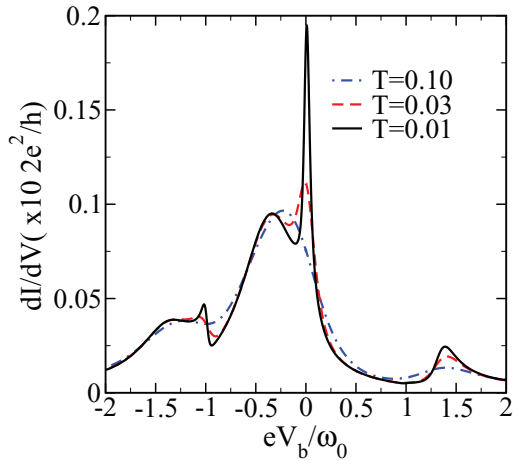


FIG. 13. (Color online) Conductance as a function of the applied bias voltage for asymmetric couplings and voltage drops (see text). Parameters are $\omega_0 = 1$, $T = 0.02$, $\tilde{E}_d^0 = -0.6$, $\Delta = 0.2$, and $\lambda = 0.7$.

splitting is clearly visible already for small bias voltages, of the order of a few times T_K/e .

In Fig. 12, we display the conductance $G = dI/dV_b$, where I is the current as a function of a applied bias voltage V_b for a temperature slightly above the Kondo temperature and several values of the electron-phonon interaction. In addition to the Kondo peak at $V_b = 0$ and the charge-transfer peak near $V_b = \pm \tilde{E}_d$, replicas of the Kondo peak with smaller intensity appear for $eV_b = \pm 2\omega_0$ reflecting the inelastic processes in which a phonon is created or destroyed. Since the curve is symmetric with respect to a change of sign of the bias voltage [$G(-V_b) = G(V_b)$], only positive V_b are shown. In general, further peaks at $eV_b = \pm 2n\omega_0$ with $n > 1$ are expected, as observed experimentally.¹⁷ These are difficult to capture within NCA due to the limitations of the numerical procedure at very low temperatures.

For experiments of transport through molecules, the couplings to the leads Γ_ν are very asymmetric in general. In Fig. 13, we show the nonequilibrium conductance for a case in which $\Gamma_L = 30\Gamma_R$ (typical of experiments with C_{60} quantum dots¹²), keeping $\Gamma_R + \Gamma_L = 2\Delta$, and the voltage drop is inversely proportional to the corresponding Γ_ν : $\mu_L = (1/31)V_b$, $\mu_R = (-30/31)V_b$. In this case, the spectral density at the molecule for finite bias voltage V_b is similar to that in which the dot is at equilibrium with the lead for which the coupling is the largest, and is not strongly modified by V_b . Since most of voltage drop falls between the system and the other lead, the situation is similar to that in scanning tunneling microscopy (STM), in which the spectral density is little affected by the less coupled lead (or STM tip) and the spectral density is reflected in the differential conductance $G(V_b)$.⁵⁷ Therefore, the resulting conductance is qualitatively similar to the spectral density as a function of frequency, shown before in Fig. 6.

V. SUMMARY AND DISCUSSION

Using the NCA, we have calculated the spectral density and nonequilibrium conductance of the Holstein-Anderson

model, which describes a molecule or a quantum dot with a singly occupied localized (magnetic) level and a single relevant phonon mode with frequency ω_0 coupled to the occupancy of the localized level. The spectral density shows interplay of the usual Kondo physics in which the magnetic moment is screened by conduction electrons at low energies, and the vibrations. As a consequence of the latter, peaks appear in the spectral density at frequencies near multiples of $\pm\omega_0$, which reflect the physics of both Kondo screening and the effect of vibrations. However, the nature of these replicas of the Kondo effect, its exact position, and width deserve further study. In particular, it would be interesting to include a finite Coulomb repulsion U and study the evolution of the replicas above and below the Fermi level, as the model evolves from the symmetric Anderson model to infinite U .

The characteristic energy scale T_K decreases slightly (not in an exponential form) with increasing electron-phonon coupling λ for fixed effective level energy \tilde{E}_d . We find that this effective level \tilde{E}_d is slightly larger than $\tilde{E}_d^0 = E_d - \lambda^2/\omega_0$ and this difference has important consequences, for example, when the Kondo temperature for different λ is compared.

The conductance through the system at small temperatures shows not only a central peak at small applied bias voltages V_b due to the Kondo peak, but also additional peaks that correspond to inelastic processes involving creation and destruction of phonons. In our calculation, for a symmetric voltage drop we only see marked peaks near $\omega = \pm 2\omega_0$, but additional peaks are expected for larger λ or smaller temperatures.

We have limited our calculations to $\lambda < 0.7$. We do not expect the NCA to be valid for large λ . For small λ , the NCA is of course valid because it reduces to second-order perturbation theory in λ . For the extreme polaronic regime $\lambda \gg 1$ at equilibrium, other techniques should be used,^{22–25,29} such as NRG. The nonequilibrium problem is more difficult and few alternative approaches exist, as discussed in the Introduction.

ACKNOWLEDGMENTS

We thank CONICET from Argentina for financial support. P.R. is sponsored by Escuela de Ciencia y Tecnología, Universidad Nacional de San Martín. This work was partially supported by PIP 11220080101821 of CONICET and PICT R1776 of the ANPCyT, Argentina.

APPENDIX: VARIATIONAL ESTIMATE OF THE EFFECTIVE LEVEL ENERGY

In this appendix, we describe our estimate of the renormalized energy level \tilde{E}_d using a simple variational wave function

$$|\psi\sigma\rangle = A \left\{ |\psi_{d\sigma}\rangle |0_\beta\rangle + \sum_K \alpha_K |\psi_{K\sigma}\rangle |0_a\rangle \right\}, \quad (\text{A1})$$

where $|\psi_{d\sigma}\rangle = d_\sigma^\dagger |F\rangle$, $|\psi_{K\sigma}\rangle = c_{K\sigma}^\dagger |F\rangle$, $|F\rangle$ is the filled Fermi sea of conduction electrons, $c_{K\sigma}^\dagger$ ($K = \nu k$) creates a conduction state above the Fermi energy, and $|0_a\rangle$ is the

vacuum of phonons a ($a|0_a\rangle = 0$) while $|0_\beta\rangle$ is the vacuum of a displaced phonon defined by $\beta^\dagger = a^\dagger + c$, where c is a real variational parameter, like A and α_K , which will be determined by minimizing the energy.

Note that this wave function, in contrast to that proposed by Varma and Yafet (VY),⁵⁶ is not a singlet but a doublet. While the VY choice leads to an energy gain of the order of the Kondo temperature, which depends exponentially on the hybridization V_K , and the correct spin ($S = 0$) of the ground state, our doublet gains more energy, with a difference proportional to $|V_K|^2$ in the Kondo limit. In this limit, a comparison of the local occupation $\langle n_d \rangle = \partial E / \partial E_d$, where E is the total energy, with NRG results suggests that the energy gain is qualitatively correct (about half the correct value) and much better than that predicted by the slave-boson approximation in mean-field level.⁵⁹

Expanding $|0_\beta\rangle = \sum_n c_n (a^\dagger)^n |0_a\rangle$ in a basis of occupations of the phonons a , using the equation $\beta|0_\beta\rangle = (a - c)|0_\beta\rangle = 0$, it is easy to see that $\langle 0_a|0_\beta\rangle = \exp(-c^2/2)$. Using this and minimizing $\langle \psi_\sigma | H | \psi_\sigma \rangle - E(\langle \psi_\sigma | \psi_\sigma \rangle - 1)$ with respect to A one obtains

$$E = \frac{\langle \psi_\sigma | H | \psi_\sigma \rangle}{\langle \psi_\sigma | \psi_\sigma \rangle} = E_F + E_d + 2\lambda c + \omega_0 c^2 + 2e^{-c^2/2} \sum_K \alpha_K V_K + \sum_K \alpha_K^2 (E_F + \epsilon_K - E), \quad (\text{A2})$$

where E_F is the energy of $|F\rangle$.

Minimization with respect to α_K and c leads to

$$\alpha_K = -\frac{V_K e^{-c^2/2}}{E_F + \epsilon_K - E}, \quad (\text{A3})$$

$$c = -\frac{\lambda}{\omega_0 - e^{-c^2/2} \sum_K \alpha_K V_K}.$$

Using the first equation to eliminate α_K , assuming for simplicity constant $V_K = V$, constant density of conduction states ρ extending up to $\epsilon_F + D$, and calling $\Delta = \pi\rho V^2$, one obtains the following system of equations:

$$c = -\frac{\lambda}{\omega_0 + e^{-c^2} \gamma(\epsilon)}, \quad \epsilon = 2\lambda c + \omega_0 c^2 - e^{-c^2} \gamma(\epsilon), \quad (\text{A4})$$

where we have defined $\epsilon = E - E_F - E_d$, $\gamma(\epsilon) = (\Delta/\pi) \ln|1 - D/(E_d + \epsilon)|$.

After solving the system, using Eq. (6) and taking into account that in the Kondo limit the significant α_K are those with ϵ_K very near ϵ_F , we can write

$$\tilde{E}_d = \langle \psi_{d\sigma} | \langle 0_b | H | 0_b \rangle | \psi_{d\sigma} \rangle - \langle \psi_{K\sigma} | \langle 0_a | H | 0_a \rangle | \psi_{K\sigma} \rangle, \quad (\text{A5})$$

with $K = K_F$ on the Fermi shell. The result can be written as

$$\tilde{E}_d = E_d - \frac{\lambda^2}{\omega_0} (2\tilde{c} - \tilde{c}^2), \quad (\text{A6})$$

where $\tilde{c} = -\omega_0 c / \lambda$ is an adimensional number, with $0 \leq \tilde{c} \leq 1$. From the first Eq. (A4), it is clear that $\tilde{c} = 1$ for $V_K = 0$ as expected.

¹A. Nitzan and M. A. Ratner, *Science* **300**, 1384 (2003).

²L. Venkataraman, J. E. Klare, C. Nuckolls, M. S. Hybertsen, and M. L. Steigerwald, *Nature (London)* **442**, 904 (2006).

³M. Galperin, M. A. Ratner, A. Nitzan, and A. Troisi, *Science* **319**, 1056 (2008).

⁴S. J. van der Molen and P. Liljeroth, *J. Phys.: Condens. Matter* **22**, 133001 (2010).

⁵J. C. Cuevas and E. Scheer, *Molecular Electronics: An Introduction to Theory and Experiment* (World Scientific, Singapore, 2010).

⁶J. Park, A. N. Pasupathy, J. I. Goldsmith, C. Chang, Y. Yaish, J. R. Petta, M. Rinkoski, J. P. Sethna, H. D. Abruña, P. L. McEuen, and D. C. Ralph, *Nature (London)* **417**, 722 (2002).

⁷W. Lian, M. P. Shores, M. Bockrath, J. R. Long, and H. Park, *Nature (London)* **417**, 725 (2002).

⁸E. A. Osorio, K. O'Neill, M. Wegewijs, N. Stuhr-Hansen, J. Paaske, T. Bjornholm, and H. S. J. van der Zant, *Nano Lett.* **7**, 3336 (2007).

⁹I. Fernández-Torrente, K. J. Franke, and J. I. Pascual, *Phys. Rev. Lett.* **101**, 217203 (2008).

¹⁰N. Roch, S. Florens, V. Bouchiat, W. Wernsdorfer, and F. Balestro, *Nature (London)* **453**, 633 (2008).

¹¹J. J. Parks, A. R. Champagne, T. A. Costi, W. W. Shum, A. N. Pasupathy, E. Neuscamman, S. Flores-Torres, P. S. Cornaglia, A. A. Aligia, C. A. Balseiro, G. K.-L. Chan, H. D. Abruña, and D. C. Ralph, *Science* **328**, 1370 (2010).

¹²S. Florens, A. Freyn, N. Roch, W. Wernsdorfer, F. Balestro, P. Roura-Bas, and A. A. Aligia, *J. Phys.: Condens. Matter* **23**, 243202 (2011).

¹³D. E. Logan, C. J. Wright, and M. R. Galpin, *Phys. Rev. B* **80**, 125117 (2009).

¹⁴P. Roura-Bas and A. A. Aligia, *Phys. Rev. B* **80**, 035308 (2009).

¹⁵P. Roura-Bas and A. A. Aligia, *J. Phys.: Condens. Matter* **22**, 025602 (2010).

¹⁶H. Park, J. Park, A. K. L. Lim, E. H. Anderson, A. P. Alivisatos, and P. L. McEuen, *Nature (London)* **407**, 57 (2000).

¹⁷N. B. Zhitenev, H. Meng, and Z. Bao, *Phys. Rev. Lett.* **88**, 226801 (2002).

¹⁸M. Berthe, A. Urbieta, L. Perdigo, B. Grandidier, D. Deresmes, C. Delerue, D. Stievenard, R. Rurali, N. Lorente, L. Magaud, and P. Ordejon, *Phys. Rev. Lett.* **97**, 206801 (2006).

¹⁹M. Galperin, M. A. Ratner, and A. Nitzan, *J. Phys.: Condens. Matter* **19**, 103201 (2007).

²⁰S. Ballmann, R. Härtle, P. B. Coto, M. Elbing, M. Mayor, M. R. Bryce, M. Thoss, and H. B. Weber, *Phys. Rev. Lett.* **109**, 056801 (2012).

²¹L. H. Yu, Z. K. Keane, J. W. Ciszek, L. Cheng, J. M. Tour, T. Baruah, M. R. Pederson, and D. Natelson, *Phys. Rev. Lett.* **95**, 256803 (2005).

²²P. S. Cornaglia, G. Usaj, and C. A. Balseiro, *Phys. Rev. B* **76**, 241403(R) (2007).

²³A. C. Hewson and D. Meyer, *J. Phys.: Condens. Matter* **14**, 427 (2002).

²⁴P. S. Cornaglia, H. Ness, and D. R. Grempel, *Phys. Rev. Lett.* **93**, 147201 (2004).

- ²⁵L. Arrachea and M. J. Rozenberg, *Phys. Rev. B* **72**, 041301 (2005).
- ²⁶M. D. Núñez Regueiro, P. S. Cornaglia, G. Usaj, and C. A. Balseiro, *Phys. Rev. B* **76**, 075425 (2007).
- ²⁷H.-C. Yong, K.-H. Yang, and G.-S. Tian, *Commun. Theor. Phys.* **48**, 1107 (2007).
- ²⁸A. Martin-Rodero, A. Levy Yeyati, F. Flores, and R. C. Monreal, *Phys. Rev. B* **78**, 235112 (2008).
- ²⁹R. C. Monreal and A. Martin-Rodero, *Phys. Rev. B* **79**, 115140 (2009).
- ³⁰J. König, H. Schoeller, and G. Schön, *Phys. Rev. Lett.* **76**, 1715 (1996).
- ³¹J. Paaske and K. Flensberg, *Phys. Rev. Lett.* **94**, 176801 (2005).
- ³²M. Galperin, A. Nitzan, and M. A. Ratner, *Phys. Rev. B* **76**, 035301 (2007).
- ³³J. E. Han, *Phys. Rev. B* **81**, 113106 (2010).
- ³⁴K. H. Yang, Y. P. Wu, and Y. L. Zhao, *Europhys. Lett.* **89**, 37008 (2010).
- ³⁵A. Goker, *J. Phys.: Condens. Matter* **23**, 125302 (2011).
- ³⁶R. C. Monreal, F. Flores, and A. Martin-Rodero, *Phys. Rev. B* **82**, 235412 (2010).
- ³⁷A. Levy Yeyati, A. Martin-Rodero, and F. Flores, *Phys. Rev. Lett.* **71**, 2991 (1993).
- ³⁸A. A. Aligia, *Phys. Rev. B* **74**, 155125 (2006).
- ³⁹N. S. Wingreen and Y. Meir, *Phys. Rev. B* **49**, 11040 (1994).
- ⁴⁰M. H. Hettler, J. Kroha, and S. Hershfield, *Phys. Rev. B* **58**, 5649 (1998).
- ⁴¹T. A. Costi, J. Kroha, and P. Wölfle, *Phys. Rev. B* **53**, 1850 (1996).
- ⁴²P. Roura-Bas, *Phys. Rev. B* **81**, 155327 (2010).
- ⁴³A. Oguri, *J. Phys. Soc. Jpn.* **74**, 110 (2005).
- ⁴⁴A. A. Aligia, *J. Phys.: Condens. Matter* **24**, 015306 (2012); references therein; arXiv:1302.4069.
- ⁴⁵R. Van Roermund, S. Y. Shiau, and M. Lavagna, *Phys. Rev. B* **81**, 165115 (2010).
- ⁴⁶L. Vaugier, A. A. Aligia, and A. M. Lobos, *Phys. Rev. B* **76**, 165112 (2007).
- ⁴⁷A. Freyn and S. Florens, *Phys. Rev. Lett.* **107**, 017201 (2011).
- ⁴⁸A. C. Hewson, *The Kondo Problem to Heavy Fermions* (Cambridge, University Press, Cambridge, UK, 1993).
- ⁴⁹L. Tosi, P. Roura-Bas, A. M. Llois, and A. A. Aligia, *Phys. B (Amsterdam)* **407**, 3263 (2012).
- ⁵⁰For nonvanishing V_K in the Kondo regime, the antiadiabatic approximation is expected to be valid when $\Gamma_\nu \ll \omega_0$, where Γ_ν are defined in Eqs. (13).
- ⁵¹D. C. Langreth, *Phys. Rev. B* **1**, 471 (1970).
- ⁵²G. D. Mahan, *Many Particle Physics* (Kluwer/Plenum, New York, 2000).
- ⁵³E. M. Lifshitz and A. L. Pitaevskii, *Physical Kinetics* (Pergamon, Oxford, 1981).
- ⁵⁴Y. Meir and N. S. Wingreen, *Phys. Rev. Lett.* **68**, 2512 (1992).
- ⁵⁵A. P. Jauho, N. S. Wingreen, and Y. Meir, *Phys. Rev. B* **50**, 5528 (1994).
- ⁵⁶C. M. Varma and Y. Yafet, *Phys. Rev. B* **13**, 2950 (1976).
- ⁵⁷A. A. Aligia and A. M. Lobos, *J. Phys.: Condens. Matter* **17**, S1095 (2005).
- ⁵⁸F. D. M. Haldane, *Phys. Rev. Lett.* **40**, 416 (1978).
- ⁵⁹Y. Wang, X. Hu, X. Xu, B. Cheng, and D. Zhang, *Phys. Rev. B* **68**, 165106 (2003).